Journal of Applied Polymer Science

Prediction of Residual Stresses and Distortion in Carbon Fiber-Epoxy Composite Parts Due to Curing Process Using Finite Element Analysis

Behrouz Tavakol, Pooneh Roozbehjavan, Ashraf Ahmed, Rony Das, Ronald Joven, Hoda Koushyar, Alejandro Rodriguez, Bob Minaie

Department of Mechanical Engineering, Wichita State University, Wichita, Kansas 67260

Correspondence to: B. Minaie (E-mail: bob.minaie@wichita.edu)

ABSTRACT: To predict the final geometry of carbon fiber-epoxy composite parts, a methodology is introduced that takes into account cure kinetics, cure shrinkage, thermal strains, tool-part interface, and development of mechanical properties during cure. These parameters affect process-induced residual stresses and distortion in the parts. A module was developed for each mechanism and a fully 3D coupled thermomechanical finite element analysis was utilized. To validate the simulation results, a square composite panel was fabricated and its pattern of distortion was obtained. The simulated distortion pattern agreed well with the actual pattern obtained from the experiments. Parallel processing and optimization of the developed codes were used resulting in 94% reduction in the computational time. The proposed methodology proved to be accurate and time-efficient in predicting the final geometry of the parts. © 2012 Wiley Periodicals, Inc. J. Appl. Polym. Sci. 000: 000–000, 2012

KEYWORDS: composites; curing; residual stress; deformation; finite element analysis

Received 7 November 2011; accepted 17 May 2012; published online

DOI: 10.1002/app.38075

INTRODUCTION

Carbon fiber-epoxy composite parts are used for a variety of applications because of their superior mechanical properties and high strength-to-weight ratio. To achieve more consistent mechanical properties, preimpregnated layers (prepregs) consisting of sheets of carbon fibers embedded in a partially cured epoxy resin are often used. Vacuum bagging is commonly used to manufacture the part in which the prepregs are laid on a tool (mold) and are covered by a vacuum bag. Then, the part is cured at elevated temperature and pressure.

It is imperative for the part to have accurate dimensions specified during design. However, during the cure process, several phenomena can result in residual stresses that can cause distortion in the part upon removal from the tool.[1,2] Such distorted parts must undergo a costly repair or be rejected. Prediction of the final part distortion is usually done in industry by a trial-and-error procedure, which is inaccurate, time-consuming, and costly. Instead, finite element analysis (FEA) can be used to accurately predict the final geometry of the composite parts by calculating the residual stresses.

Different mechanisms affect the residual stresses during cure.[3,4] The first one is due to inherent anisotropy in composite materials. For example, this is evident by directional dependence of the coefficient of thermal expansion (CTE) of composites where the CTE in resin-dominated direction is much higher than fiber-dominated direction.[5] This difference in CTE can aggravate residual stresses and dimensional inaccuracy during ramp-up and cooldown in the cure process.

Resin chemical shrinkage is another mechanism that can cause residual stresses in polymer composites.[6] The resin polymerizes and shrinks during cure, generating dimensional changes.[7] Shrinkage is more pronounced in resin-dominated direction of the material than in fiber-dominated direction.[1] In addition to resin chemical shrinkage, resin flow (bleeding),[8,9] and compaction[10,11] are two other parameters causing a composite part to shrink. During the cure process, excess resin flows out causing nonuniform distribution of fiber volume fraction which is another source of inducing residual stress.[12] The compaction is usually not uniform through the thickness and contributes more to the outermost layers of the laminate, making the plies thin at the top and thick at the bottom.[13] Therefore, cure shrinkage contains the effect of resin chemical shrinkage, resin flow, and compaction.

Another mechanism that can generate residual stress is the interaction between the tool and the part during heating and cooling cycles in the cure process.[14] Aluminum and steel tools

have much higher CTE than composite laminates. As the tool expands during ramp-up, it stretches the plies closest to it due to frictional forces between the tool and the part.[15] As the cure cycle progresses and the resin cures, the plies are locked in a stretched position due to resin solidification. This generates a nonuniform strain distribution in the through-thickness direction causing bending moment upon cooling of the part.[16] When the laminate is thick, temperature and degree of cure (DOC) gradients are other significant sources of process-induced residual stresses.[17,18]

In spite of unique advantages of using FEA instead of trial-and-error procedures in estimating distortion and residual stresses, the FEA has its own limitations. Because of the complexity of the curing process and the presence of several mechanisms inducing residual stresses, the FEA has usually been used to estimate distortion and residual stresses in simple shapes. Because of several nonlinearities associated with geometry, material properties, and boundary conditions, significant computational time has been required to perform FEA even when using a 2D analysis. In this regard, some researchers have presented process models in which only some of the mechanisms causing residual stress were included and a simplified finite element method (FEM) or finite difference method (FDM) was employed.[1,4,19–22]

White and Hahn[19] presented LamCure model containing cure kinetics and residual stress modules. They used a linear viscoelastic model in the residual stress module and thermal strain was considered to be significantly lower than chemical shrinkage. The use of this 2D model was limited to thin composite laminates. Bogetti and Gillespie[1] introduced a process model in which a continuous fiber micromechanics model was utilized to estimate lamina properties from the properties of its constituents (fiber and resin) but the effect of fiber-matrix interface was neglected. Johnston et al.[6] developed a 2D model that included chemical shrinkage, CTE mismatch, tool-part interface, and resin flow. A plane strain approach was considered and tool-part interface was modeled using a shear layer.

This study addresses the shortcomings of the previous studies by making contributions in the following three areas. First, a fully 3D coupled thermomechanical process model is introduced that can accurately predict process-induced residual stresses and consequent distortion. It will be shown later in this article that it is necessary to use a 3D model to obtain some of the results to be presented.

Second, the 3D process model presented also considers the most important mechanisms that induce residual stresses during cure including (1) cure kinetics, (2) nonlinear orthotropic chemical cure shrinkage, (3) uniform orthotropic resin flow, (4) uniform through-thickness compaction, (5) changes in nonlinear orthotropic thermal and mechanical properties due to curing, (6) nonlinear mechanical and thermal contacts at tool-part interface, and (7) different nonlinear orthotropic CTE models for during cure and after cure.

Third, ply properties are directly measured using unique contemporary methods and are incorporated into the simulation. By considering the effect of the fiber matrix interface, this approach improves the accuracy of the material database during cure and, thus, the simulation is more accurate.

In addition, parallel processing and optimization of the developed codes are introduced that significantly reduce the computational time for 3D simulations.

TECHNICAL APPROACH

Material and Process

IM7/977-2 prepreg was used as the primary material that contains IM7 fibers preimpregnated with CYCOM 977-2 toughened epoxy resin. This resin (manufactured by Cytec Engineered Materials) has an elastic modulus of 3.5 GPa and a tensile strength of 81 MPa, formulated for press molding and autoclave processes.[23] IM7 consists of continuous carbon fiber tows with a filament diameter of about 5 μm and a moderate elastic modulus of 270 GPa.[24] In this study, unidirectional (UD) tape of IM7/977-2 was used in which carbon fibers were parallel and lying only in the longitudinal direction. The elastic modulus of a fully cured IM7/977-2 UD prepreg is about 165 GPa in the longitudinal direction and about 9 GPa in both transverse and through-thickness directions.

The manufacturer's recommended cure cycle for a thin laminate (up to 32 plies) was used which consists of a heat-up cycle with a ramp rate of 2.78°C/min to 177°C followed by a 3-h hold at that temperature. The same ramp rate was applied during cooldown. Autoclave was pressurized to 0.6 MPa with a rate of 15–35 kPa/min. The pressure was then kept constant during cure until room temperature was reached during the cooldown cycle.

Methodology

To accurately predict process-induced residual stresses and distortion, several modules were developed to input material properties and processing parameters during the cure cycle. The order of loading such modules into the simulation was also important, especially when outputs of some modules were used as inputs for others. For example, modules predicting the mechanical properties must be loaded just after the modules predicting thermal properties since several mechanical properties were related to temperature and DOC. Therefore, the procedure shown in Figure 1 was introduced to appropriately take into account all important parameters for 3D simulation of the distortion.

Cure kinetics was the first module loaded to predict the DOC. Using the cure rate, the heat flux due to the cure chemical reactions was obtained and fed into thermal analysis. Next, heat capacity and thermal conductivity were estimated. Then, heat flux from different sources such as curing and external heat flux were added to a transient thermal analysis to calculate the temperature for the current time increment. Subsequently, cure shrinkage model was loaded to predict strain arising from cure chemical shrinkage, resin flow, and compaction. This strain was later added to other strains induced by thermal and mechanical loadings. Finally, mechanical analysis was conducted to estimate the stress and other related parameters. To guarantee that the temperature, strains, and stresses were being predicted accurately, such procedure must be repeated for each time increment which implies conducting staggered coupled thermomechanical analysis with errors within one time increment.

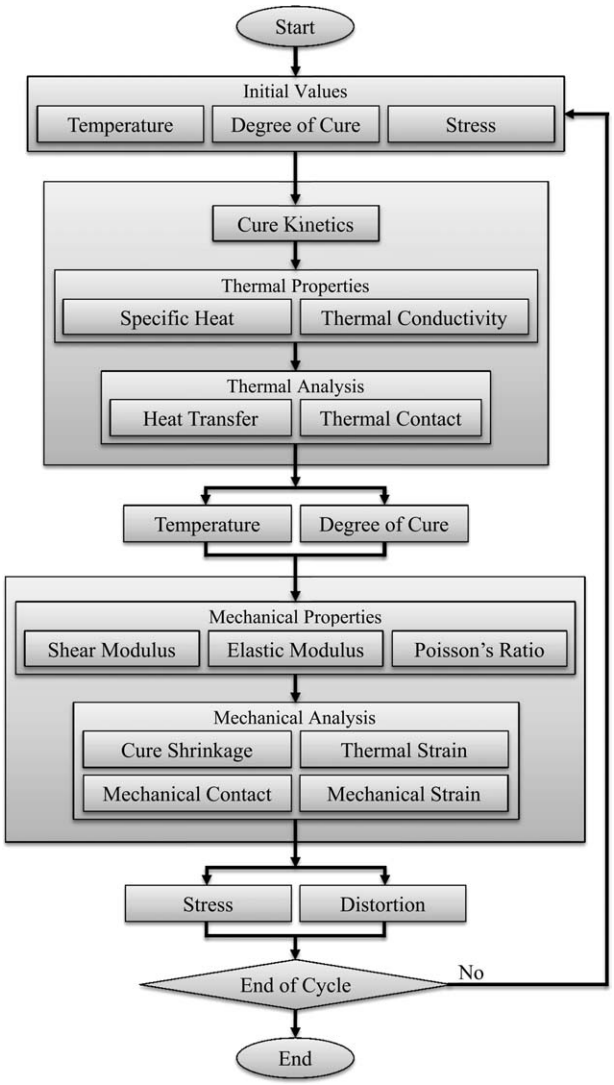

Figure 1. Proposed procedure for simulation of distortion.

Modules and Material Properties

DOC was estimated in the cure kinetics module using the Springer–Loos model [eq. (1)]:[25]

$$\frac{d\alpha}{dt} = \left(A_1 \exp\left(-\frac{\Delta E_1}{RT}\right) + A_2 \exp\left(-\frac{\Delta E_2}{RT}\right)\alpha\right)(1-\alpha)(B-\alpha) \quad (1)$$

where ΔE is the activation energy, R is the universal gas constant, T is the absolute temperature, and A_i and B are constants usually determined by curve fitting to the experiment. Based on the experimental data obtained from a differential scanning calorimeter (DSC), this model precisely followed the experiment. Using the DOC and temperature of the last increment, a FDM can be utilized to estimate the DOC for the current time increment:

$$\alpha_n = \alpha_{n-1} + (t_n - t_{n-1}) \cdot \left.\frac{d\alpha}{dt}\right|_{n-1} \quad (2)$$

where n and t are the increment number and time, respectively. Employing the FDM in FEM is typically accomplished by using one-step finite difference. This approach may work properly when time increments are small; however, the errors may not be negligible when time increments of up to several hundred seconds are used. To overcome this problem, a code was written to accurately perform a fully (multistep) FDM within each time increment of FEM.

The two required thermal properties were specific heat capacity (C_p) and thermal conductivity. The specific heat capacity was assumed to be a linear function of temperature while thermal conductivity was assumed to be constant but orthotropic. For a UD carbon fiber-epoxy prepreg, thermal conductivity in the fiber direction is approximately an order of magnitude higher than other principal directions.[26]

The cure shrinkage module estimated the resultant of three parameters including cure chemical shrinkage, resin flow, and compaction. It was assumed that the resin flow and compaction have the same trend as cure chemical shrinkage and are position-independent. Although this assumption infers uniform composite thickness, it significantly reduces the computational time. It should be noted that the resin flow and compaction usually start before chemical shrinkage and they may not have such a significant contribution to final residual stresses, especially because the material is in its low-viscosity state and the residual stresses induced in this step may vanish later due to stress relaxation.[5] A modified version of the Bogetti–Gillespie shrinkage model was used. Bogetti and Gillespie applied this model to a pure resin system and, then, they estimated the ply shrinkage using a micromechanics model. However, in this study, the model was directly used to obtain the ply shrinkage. The cure shrinkage for a particular direction was estimated using the following equation:

$$\varepsilon_i^s = C_i\left(\sqrt[3]{1+V_r^s} - 1\right) \quad (3)$$

where ε_i^s is cure shrinkage in direction i, V_r^s is volume cure shrinkage, and C_i is coefficient of directional cure shrinkage determined from experimental results using a dynamic mechanical analyzer (DMA) and a thermomechanical analyzer (TMA). The procedures to obtain those experimental values have been described in our previous study[27] and the associated parameters for this module are shown in Table I.

Another module was dedicated to estimating the coefficient of thermal expansion (CTE) and thermal strain during cure. For fully cured composites, the CTE is a nonlinear function of temperature in which the nonlinearity is observed when approaching the glass transition temperature (T_g). For uncured or partially cured composites, CTE should be determined as a function of both temperature and DOC. In addition, orthotropic behavior of the CTE for a UD composite ply had to be considered since CTE in the longitudinal direction is negative or close to zero, while CTE in transverse and through-thickness directions can be 50% higher than the CTE for aluminum.

Finally, a separate module was devoted to determine the mechanical properties during cure including elastic and shear moduli in three principal directions and Poisson's ratios in the three major planes. A TA Instruments DMA Q800 was used to

Table I. Coefficients of Directional Cure Shrinkage

Parameter	Associated property	Value
C_1	Longitudinal cure shrinkage	0.42
C_2	Transverse cure shrinkage	2.11
C_3	Through-thickness cure shrinkage	4.82
V_r^s	Total volumetric cure shrinkage	0.01

Table II. Parameters of Springer–Loos Cure Kinetics Model

Parameter	Value	Unit
A_1	2.46E+02	1/s
A_2	−4.18E-05	1/s
E_1	8.26E+04	J/mol
E_2	2.65E+04	J/mol
B	6.26E+03	-

obtain modulus development during cure in different directions and the geometry parameters of samples were properly chosen.[28] A modified Bogetti–Gillespie model was then introduced to represent the changes in mechanical properties during cure.

Finite Element Modeling

Fully 3D simulations were conducted to predict the pattern of distortion as well as the maximum value of distortion. MSC Marc 2008r1 was used to implement the developed procedure in which different modules were written in Fortran and loaded by Marc as user subroutines for each time increment. A coupled thermomechanical analysis (staggered approach) was used during the entire cure cycle. Transient heat transfer analysis was performed to consider heat of chemical reactions and to simulate heating and cooling cycles. Since a large distortion might occur during cure, the total Lagrangian approach was used to perform nonlinear mechanical analysis. In this case, stress and strain were represented as second Piola-Kirchhoff stress and Green-Lagrange strain tensors, respectively.[29] An eight-node composite brick element was used where the ply properties were imported directly as the layer properties. Each layer can have its own thickness, orientation, and material properties.[30]

A schematic of a composite panel used to simulate distortion is shown in Figure 2. The composite part was held between a tool at the bottom and a caul plate at the top. Autoclave pressure was applied on the caul plate so the composite part was indirectly subjected to pressure. Cure cycle temperature was applied to exterior faces of the tool and the caul plate through MSC Marc's Ufilm user subroutine.

To simulate the tool-part interface, two types of contacts were considered between the tool and the composite part: mechanical contact dealing with frictional forces and thermal contact for heat transfer. The Coulomb model with stick-slip behavior and nonlinear changes in the coefficient of friction, as described in our previous study,[31] was used for the mechanical contact. In the thermal contact, a threshold distance between contact surfaces was defined to activate or deactivate the heat transfer between the tool and the part.

Validation of Finite Element Modeling

First, the simulation was conducted for one element and the results of different modules were compared with the material properties and process parameters which were experimentally measured. The simulation was then conducted for a composite panel measuring 430 mm by 430 mm with a stacking sequence of $[0/45/90/-45]_4$. The asymmetric stacking sequence was intentionally selected to check the capability of the simulation to predict severe distortion. A composite panel similar to the simulated one was laid and cured in the autoclave.

A seven-axis Romer arm equipped with a laser scanner was used to measure three types of parameters: maximum distortion, 3D pattern of distortion, and pattern of thickness variation. The maximum distortion of the panel was defined as the maximum deviation of the panel from a flat reference surface when three of four corners were in contact with the reference. The 3D pattern of distortion was obtained by comparing each point of the surface with its equivalent point on the reference

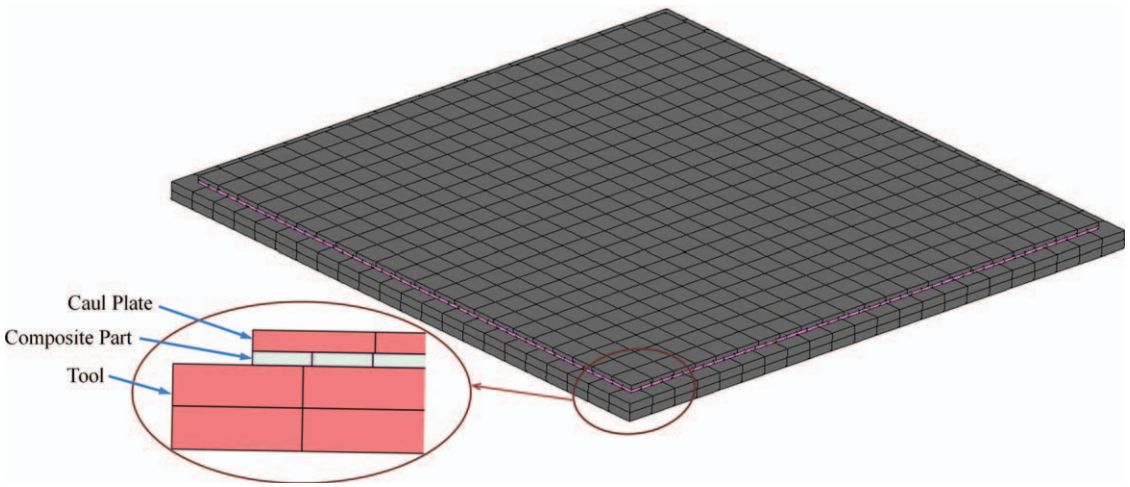

Figure 2. Schematic of a composite panel used to simulate distortion. [Color figure can be viewed in the online issue, which is available at wileyonlinelibrary.com.]

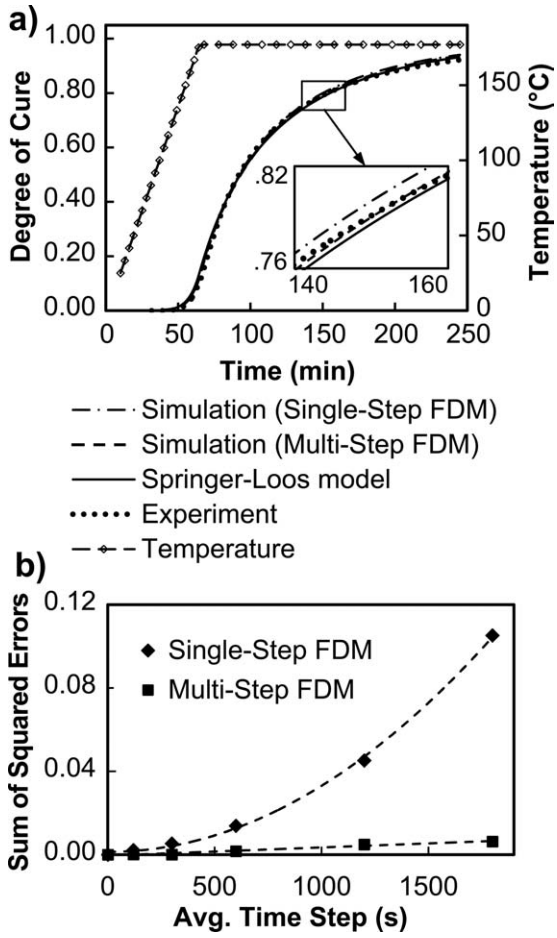

Figure 3. (a) Comparison of DOC obtained using experiment, model, and simulation; (b) comparison of errors in estimation of DOC using single-step and multistep FDM for different time steps.

surface. The panel was vertically held during scanning to minimize the effect of weight on the measured distortion.

RESULTS AND DISCUSSION

Modules and Material Properties

Parameters of the Springer–Loos model (shown in Table II) were obtained using the least squares fit method in Microsoft Excel. Figure 3(a) shows the comparison for the DOC. Both model and simulation results were in good agreement with the experiment. Since the time steps were relatively small (in the order of hundred seconds) for conducting this simulation, the difference between the single-step and the multistep FDM was not very significant. However, as shown in Figure 3(b), increasing the time step may cause a significant error in prediction of the DOC when using the single-step FDM. In other words, the multistep FDM provides a negligible error that is not greatly affected by increasing the time step. The increase in computational time for using multistep FDM is also negligible. Therefore, the multistep FDM more accurately predicts the DOC which is considered to be the most important parameter of this simulation since other modules use the DOC as an input for prediction of other parameters.

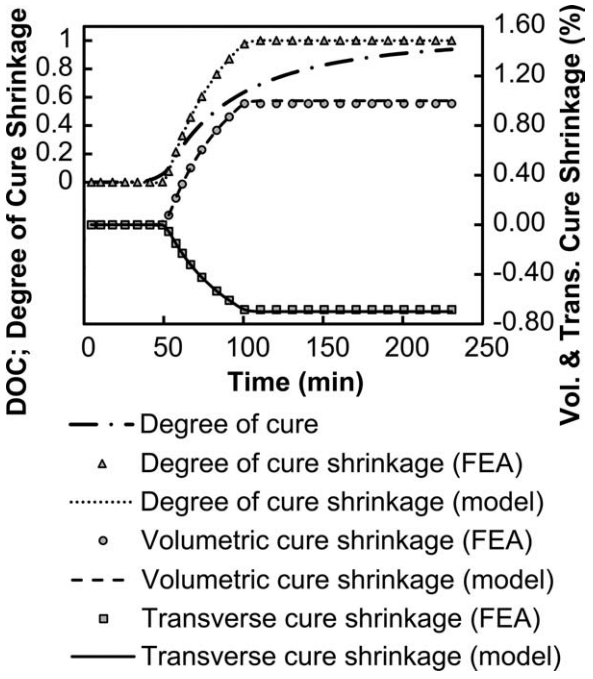

Figure 4. Comparison of cure shrinkage between Bogetti–Gillespie model and simulation results.

As shown in Figure 4, the developed code performed well in estimating cure shrinkage during cure from the simulated DOC. Cure shrinkage in the longitudinal direction was very small; however, significant cure shrinkage was observed in the transverse and through-thickness directions. These were in good agreement with the study performed by Bogetti and Gillespie.[1] Cure shrinkage in the through-thickness direction was considered to result from chemical shrinkage, resin flow, and compaction; however, for the other directions the cure shrinkage was assumed to result from only chemical shrinkage and resin flow.

The developed CTE module was used to predict the thermal strains in different directions for the orthotropic material as shown in Figure 5. Thermal strain in the longitudinal direction was negligible while the other two directions showed high thermal strain especially during ramp-up. Conversely, White and Hahn[5] considered thermal strains in both longitudinal and transverse directions to be independent of cure state. To verify

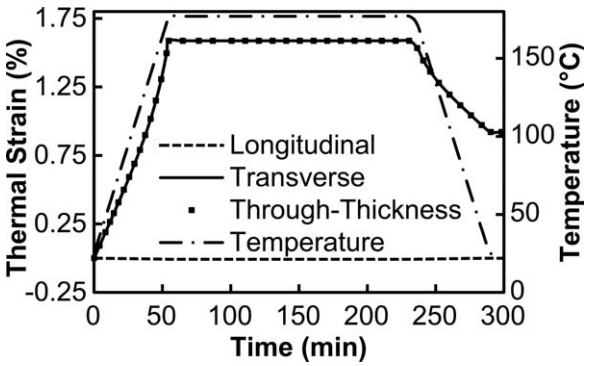

Figure 5. Thermal strain in different directions for single-ply element.

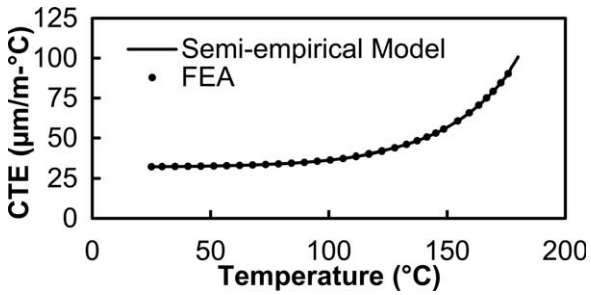

Figure 6. Comparison of CTE between semiempirical model and simulation for fully cured ply in through-thickness direction.

our CTE module, the derivative of the thermal strain with respect to temperature was used to obtain the CTE. Figure 6 shows good agreement between simulation results and semiempirical model during cooldown in the through-thickness direction. Similar agreement was also observed during different stages of curing for other directions.

Because of the similarity observed in trend of modulus development during cure for all elastic and shear moduli, the experimental results for storage modulus development in longitudinal and through-thickness directions were used as reference curves and other properties were obtained accordingly. Figure 7 shows the development of storage modulus during cure in longitudinal and trough-thickness directions for a specimen cured and tested in a DMA.

Using the DOC for the same cure cycle, the modulus development can be represented as a function of DOC (Figure 8). These data were then used to obtain the parameters of the modified Bogetti–Gillespie modulus model. The original Bogetti–Gillespie model had been used to estimate the modulus development of a resin system during cure. However, in the current study, the Bogetti–Gillespie modulus model was applied to a composite material. Using this approach, the ply properties obtained from the experiments were directly imported into the simulation. Table III shows two sets of parameters for longitudinal (fiber-dominated) and through-thickness (resin-dominated) directions. Based on the set that the property belonged to, the

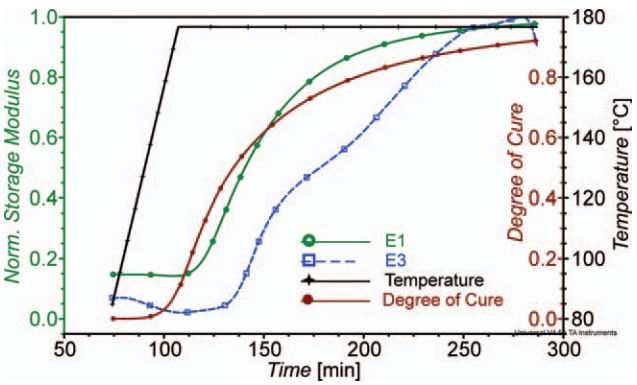

Figure 7. Storage moduli and DOC for 977-2 UD tape prepreg. [Color figure can be viewed in the online issue, which is available at wileyonlinelibrary.com.]

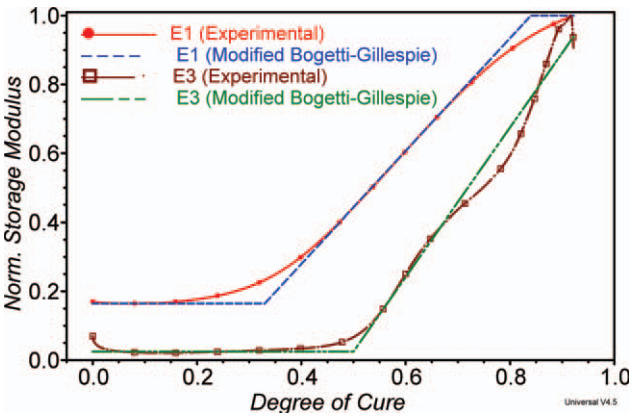

Figure 8. Storage modulus as a function of DOC. [Color figure can be viewed in the online issue, which is available at wileyonlinelibrary.com.]

properly normalized trend was selected and then scaled by the fully cured specimen property. For example, to obtain the elastic modulus in the transverse direction, the resin-rich set was used; the transverse elastic modulus for a fully cured specimen was obtained by conducting a tensile test in the transverse direction, and the normalized trend was scaled accordingly. The same procedure was utilized to obtain other elastic and shear moduli. Following mechanics of materials approach, the Poisson's ratios were also estimated.

Void volume fraction was also obtained from the center of the part according to ASTM 3171-09 and determined to be $<0.2\%$. Based on our previous study,[32] the effect of this amount of voids on the thermal and mechanical properties was neglected.

Interpretation of Simulation Results during Cure

The simulation steps were pressurization, temperature ramp-up cycle, isothermal cycle, temperature cooldown cycle, and depressurization. The von Mises stress distribution at different time increments is shown in Figure 9. Starting with zero stress at the beginning, the stress increased at earlier stages of the ramp-up cycle due to CTE mismatch between the tool and the part as well as significant CTE mismatch between different layers of the part. At later stages of the ramp-up cycle, the cure shrinkage mechanism also began when the DOC exceeded 0.05 and, consequently, the stress increased at a higher rate. At the beginning of the isothermal cycle [minute 57 in Figure 9(c)], the CTE mechanism was not effective anymore and changes in stress occurred due to storage modulus development and cure shrinkage mechanisms. As expected, this behavior had a greater effect

Table III. Parameters of Modified Bogetti–Gillespie Model for Composite Modulus Development

Model parameter	Set 1 (fiber dominant)	Set 2 (Resin dominant)
E^0	0.165	0.025
E^∞	1	1
α_{gel}	0.33	0.50
α_{diff}	0.84	0.95

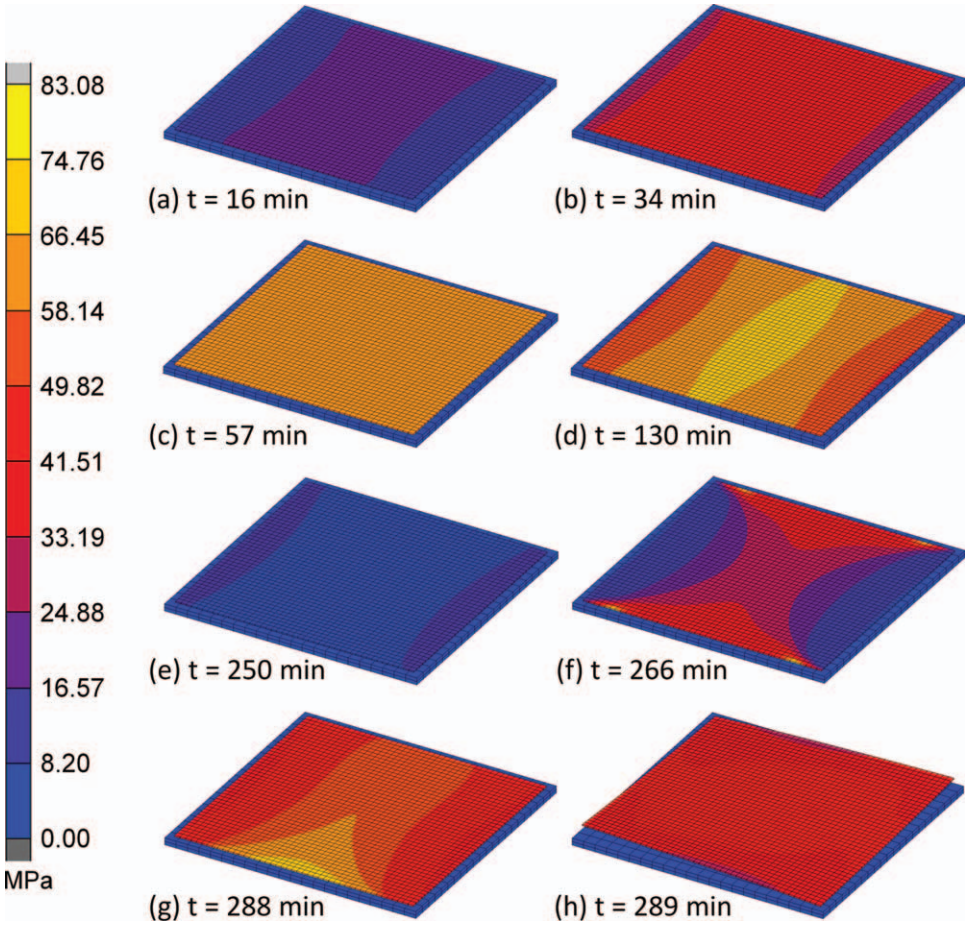

Figure 9. von Mises stress distribution during cure. [Color figure can be viewed in the online issue, which is available at wileyonlinelibrary.com.]

on the stress during earlier stages of the isothermal cycle and the effect of both mechanisms gradually diminished upon reaching the vitrification point.

During the earlier stages of the cooldown cycle [Figure 9(e)], the major active mechanism affecting stress was CTE mismatch. For this cycle, the CTE of the part was considered to be only a function of temperature and, due to its negative effect, von Mises stress showed a negative trend. Continuing on the cooldown cycle, the stress type changed and the final stress was found to be significant at lower temperatures [Figure 9(f)]. Unlike the ramp-up cycle in which the part was sticking to the tool, stick-slip behavior was attributed to the friction at the tool-part interface and, due to irregular slippage of some elements, local changes in stress pattern were observed. Figure 9(g, h) shows the stress distribution just before and after depressurizing, respectively. After the autoclave was depressurized, the part significantly distorted to reach stress equilibrium. During this stage, an active and frictionless contact was assumed

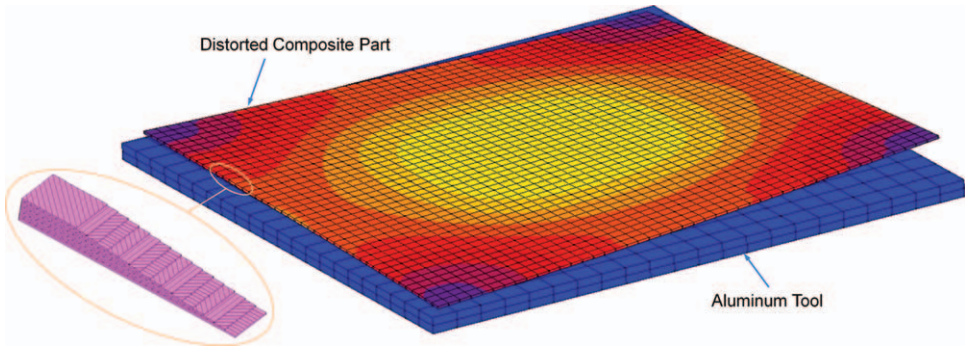

Figure 10. Simulation of distortion of panel (caul plate not shown). [Color figure can be viewed in the online issue, which is available at wileyonlinelibrary.com.]

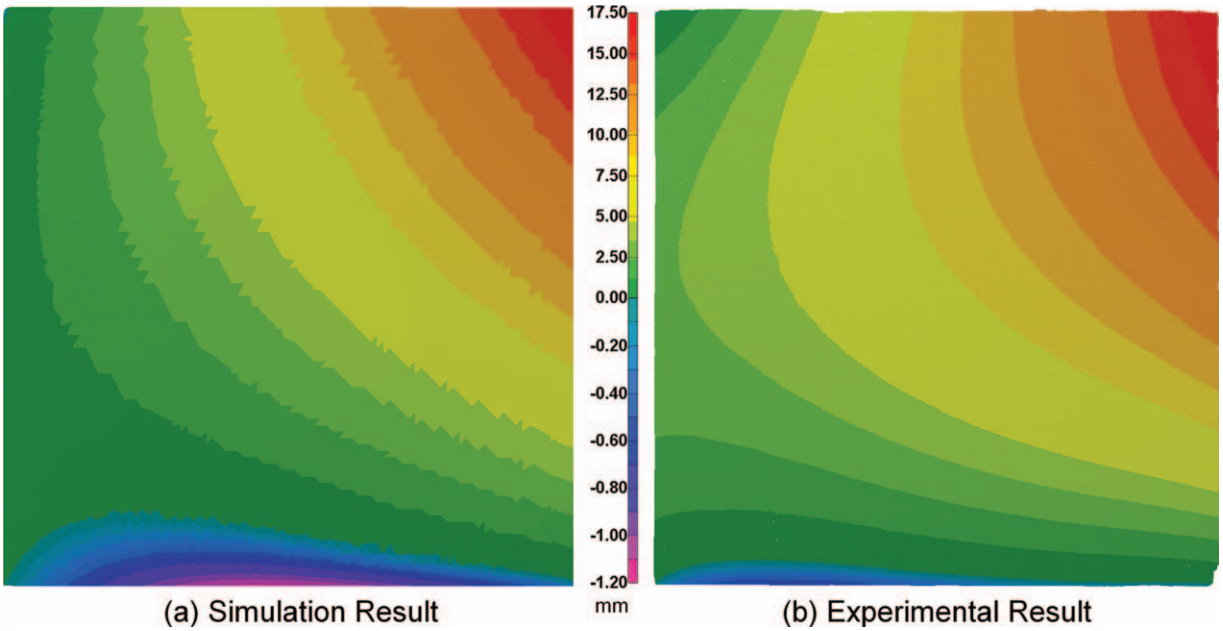

Figure 11. Comparison of distortion between (a) simulation and (b) experiment for tool side of composite panel. [Color figure can be viewed in the online issue, which is available at wileyonlinelibrary.com.]

between the tool and the cured part to let the part deform naturally on the tool.

Interpretation of Simulation Results after Cure

To correctly interpret the simulation results shown in Figure 10, a user-friendly Python code was developed to obtain the nodal information from the distorted part and then convert it to a format readable by PolyWorks.

Figure 11 shows a comparison of the simulation results with the experimental results for the tool side in PolyWorks. Good agreement was observed not only for the maximum distortions values but also for the 3D pattern of distortion. It should be noted that obtaining such a 3D pattern of distortion for the panel is feasible only by conducting a fully 3D FEA. Accurate prediction (within 2% error) of significant maximum distortion (about 17 mm) can also be considered as another proof of the ability of the simulation to correctly predict the final geometry of composite parts. The minor difference in the patterns of distortion for the simulation and the experiment can be contributed to two major sources. First, there is always an unavoidable error

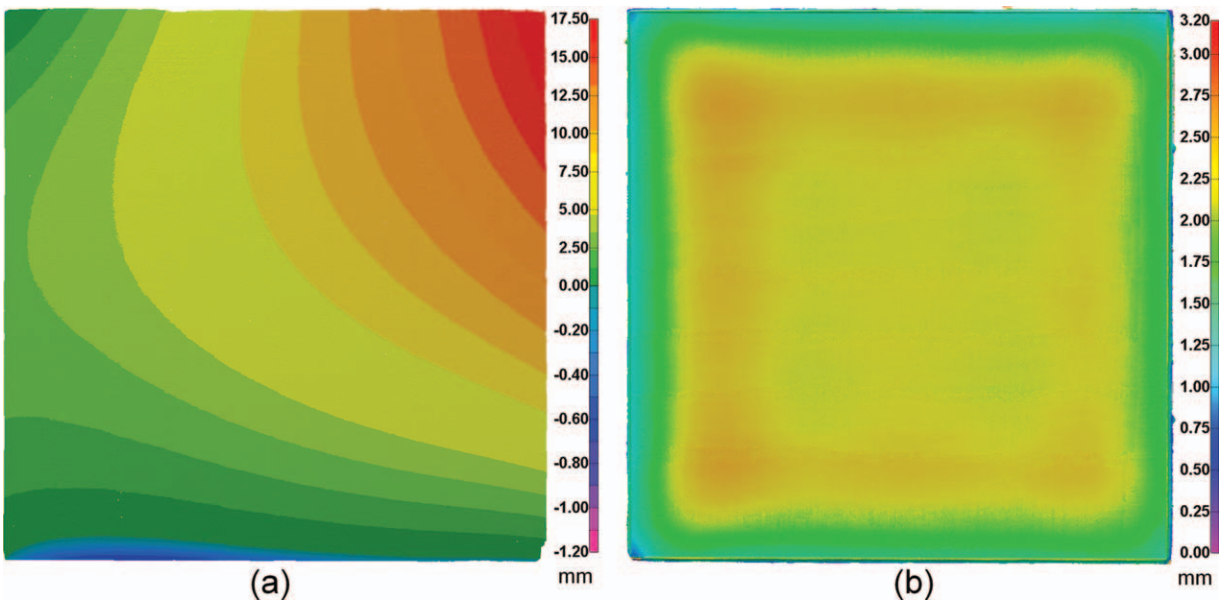

Figure 12. Fabricated panel: (a) 3D pattern of distortion for bag side and (b) pattern of thickness variation. [Color figure can be viewed in the online issue, which is available at wileyonlinelibrary.com.]

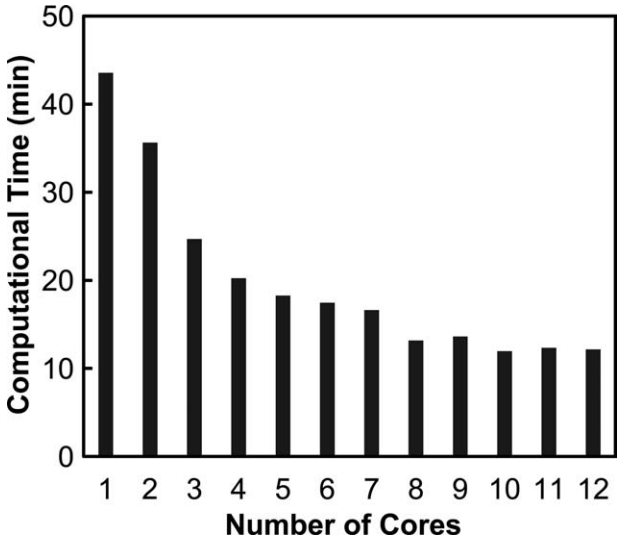

Figure 13. Parallel processing: reducing the computational time by increasing the number of cores.

associated with numerical solutions. This type of error can be reduced by choosing smaller time steps for simulation; however, this can dramatically increase the computational time. Another major source of error can be due to deviation from the actual manufacturing process such as temperature, pressure, and vacuum fluctuations inside the autoclave or presence of defects and voids in the fabricated panel. In addition to the tool side, the bag side pattern of distortion and pattern of thickness variation were experimentally obtained (Figure 12).

Parallel Processing

Using parallel processing and optimization of the developed Fortran codes, the computational time was reduced by 94%. Generally, using more cores is expected to lower the computational time. However, in this study, increasing the number of cores beyond a certain number did not lead to a significant reduction in the computational time in our simulations (Figure 13). Therefore, there is an optimum number of cores in which parallel processing can save time. Under this optimum condition, large matrices are broken into smaller matrices while the duplicated interdomain nodes do not significantly increase the computational time and that communication between different domains is not excessive. Finally, this study showed that, by decomposing a domain appropriately, the accuracy of the simulation results are not affected by the number of cores used.

CONCLUSIONS

In this article, a fully 3D coupled thermomechanical FEA was presented to predict the process-induced residual stresses and distortion. Complex mechanical and thermal contacts were considered at the tool-part interface and at the caul plate-part interface. Nonlinearities in the DOC, cure shrinkage, coefficient of thermal expansion, and development of mechanical properties during cure were incorporated into the simulation. Ply properties were directly obtained, modeled, and imported into the simulation instead of measuring fiber and resin properties and using micromechanics models. This approach improved the accuracy of during-cure properties by considering the effect of fiber-resin interface during the entire cure cycle.

A square composite panel was fabricated to validate the simulations. Methods were developed to compare the experimental and simulated patterns of distortion. Good agreement between the simulation and experimental results for maximum distortion and 3D pattern of distortion was obtained. Parallel processing was used along with optimization of the codes that resulted in reducing the computational time by 94%.

ACKNOWLEDGMENTS

The authors thank financial support from the National Aeronautics and Space Administration (Grant No. NNX09AO58A).

REFERENCES

1. Bogetti, T. A.; Gillespie, J. W., Jr. *J. Compos. Mater.* **1992,** *26*, 626.
2. Hahn, H. T. *J. Compos. Mater.* **1976,** *10*, 266.
3. White, S. R.; Kim, Y. K. *Mech. Compos. Mater. Struct.* **1998,** *5*, 153.
4. Wisnom, M. R.; Gigliotti, M.; Ersoy, N.; Campbell, M.; Potter, K. D. *Compos. Part A: Appl. Sci. Manuf.* **2006,** *37*, 522.
5. White, S. R.; Hahn, H. T. *J. Compos. Mater.* **1992,** *26*, 2423.
6. Johnston, A.; Vaziri, R.; Poursartip, A. *J. Compos. Mater.* **2001,** *35*, 1435.
7. Shah, D. U.; Schubel, P. J. *Polym. Test.* **2010,** *29*, 629.
8. Dave, R.; Kardos, J. L.; Dudukovic, M. P. *Polym. Compos.* **1987,** *8*, 29.
9. Hubert, P.; Vaziri, R.; Poursartip, A. *Int. J. Numer. Methods Eng.* **1999,** *44*, 1.
10. Gutowski, T. G.; Morigaki, T.; Cai, Z. J. *Compos. Mater.* **1987,** *21*, 172.
11. Min, L.; Yanxia, L.; Zuoguang, Z.; Yizhuo, G. *Polym. Compos.* **2008,** *29*, 560.
12. Hubert, P.; Poursartip, A. J. *Reinf. Plast. Compos.* **1998,** *17*, 286.
13. Darrow, D. A., Jr.; Smith, L. V. *J. Compos. Mater.* **2002,** *36*, 2407.
14. Twigg, G.; Poursartip, A.; Fernlund, G. *Compos. Sci. Technol.* **2003,** *63*, 1985.
15. Ersoy, N.; Potter, K.; Wisnom, M. R.; Clegg, M. J. *Compos. Part A: Appl. Sci. Manuf.* **2005,** *36*, 1536.
16. Twigg, G.; Poursartip, A.; Fernlund, G. *Compos. Part A: Appl. Sci. Manuf.* **2004,** *35*, 135.
17. Bogetti, T. A.; Gillespie, J. W. *J. Compos. Mater.* **1991,** *25*, 239.
18. Guo, Z.-S.; Du, S.; Zhang, B. *Compos. Sci. Technol.* **2005,** *65*, 517.
19. White, S. R.; Hahn, H. T. *J. Compos. Mater.* **1992,** *26*, 2402.
20. Rabearison, N.; Jochum, C.; Grandidier, J. C. *Comput. Mater. Sci.* **2009,** *45*, 715.

21. Chapman, T. J.; Gillespie, J. W.; Pipes, R. B.; Manson, J.-A. E.; Seferis, J. C. *J. Compos. Mater.* **1990,** *24*, 616.
22. Yan, X. J. *Appl. Polym. Sci.* **2007,** *103*, 2310.
23. Cytec Eng. Materials, Cycom 977-2 Datasheet. Available at: http://cytec.com/engineered-materials/products/Datasheets/CYCOM%20977-2.pdf. Accessed on January 25, **2012.**
24. Hexcel, HexTow(R) Carbon Fiber. Available at: http://www.hexcel.com/Resources/SelectorGuides/CarbonFiber_SelectorGuide_us.pdf. Accessed on January 25, **2012.**
25. Lee, W. I.; Loos, A. C.; Springer, G. S. *J. Compos. Mater.* **1982,** *16*, 510.
26. Johnston, A. An Integrated Model of the Development of Process-Induced Deformation in Autoclave Processing of Composite Structures. Ph.D. Thesis. The University of British Columbia, Vancouver, BC, Canada, April 1997.
27. Das, R.; Tavakol, B.; Ahmed, A.; Minaie, B. In *Proceedings of International SAMPE Symposium, and Exhibition*, Long Beach, CA, May 23–26, **2011.**
28. Tavakol, B.; Das, R.; Ahmed, A.; Rodriguez, A.; Minaie, B. In *Proceedings of International SAMPE Symposium and Exhibition*, Seattle, WA, May 17–20, **2010.**
29. MSC Marc 2008 r1, Manual Volume A: Theory and User Information.
30. MSC Marc 2008 r1, Manual Volume B: Element Library.
31. Joven, R.; Tavakol, B.; Rodriguez, A.; Minaie, B. In *Proceedings of International SAMPE Symposium and Exhibition*, Seattle, WA, May 17–20, **2010.**
32. Koushyar, H.; Alavi-Soltani, S.; Minaie, B.; Violette, M. *J. Compos. Mater.*, to appear.